Computational Statistics and Data Analysis 58 (2013) 45–57

Contents lists available at SciVerse ScienceDirect

Computational Statistics and Data Analysis

journal homepage: www.elsevier.com/locate/csda

Extracting common pulse-like signals from multiple ice core time series

Julien Gazeaux [a], Deborah Batista [b], Caspar M. Ammann [c], Philippe Naveau [d,*], Cyrille Jégat [e], Chaochao Gao [f]

[a] Laboratoire Atmosphères, Milieux, Observations Spatiales (LATMOS), IPSL, UPMC, UVSQ, CNRS/INSU, Paris, France
[b] Department of Mathematical Sciences, University of Colorado Denver, Denver, CO, USA
[c] Climate Science Applications Program, Research Applications Laboratory, NCAR, Boulder, CO, USA
[d] Laboratoire des Sciences du Climat et l'Environnement, IPSL-CNRS, Gif-sur-Yvette, France
[e] Ecole Nationale Supérieure des Mines de Paris, Paris, France
[f] Department of Environmental Sciences, Rutgers University, New Brunswick, NJ, USA

ARTICLE INFO

Article history:
Received 16 April 2010
Received in revised form 30 January 2012
Accepted 31 January 2012
Available online 7 February 2012

Keywords:
Signal extraction
Multiprocess Kalman filter
Volcanic eruptions
Pulse-like signals
Climate forcing

ABSTRACT

To understand the nature and cause of natural climate variability, it is important to possess an accurate estimate of past climate forcings. Direct measurements that are reliable only exist for the past few decades. Therefore knowledge of prior variations has to be established based on indirect information derived from natural archives. The challenge has always been to find a strict objective method that can identify volcanic events and offer sound amplitude estimates in these noisy records. An automatic procedure is introduced here to estimate the magnitude of strong, but short-lived, volcanic signals from a suite of polar ice core series. Rather than treating records from individual ice cores separately and then averaging their respective magnitudes, our extraction algorithm jointly handles multiple time series to identify their common, but hidden, volcanic pulses. The statistical procedure is based on a multivariate multi-state space model. Exploiting the joint fluctuations, it provides an accurate estimator of the timing, peak magnitude and duration of individual pulse-like deposition events within a set of different series. This ensures a more effective separation of the real signals from spurious noise that can occur in any individual time series, and thus a higher sensitivity to identify smaller scale events. At the same time, it provides a measure of confidence through the posterior probability for each pulse-like event, indicating how well a pulse can be recognized against the background noise. The flexibility and robustness of our approach, as well as important underlying assumptions and remaining limitations, are discussed by applying our method to first simulated and then real world ice core time series.

1. Introduction

1.1. Records of volcanic eruptions

Explosive volcanic eruptions are extreme events that can inject large amounts of sulfur-baring gases into the stratosphere. There, the gases are converted into small sulfuric acid droplets that spread and blanket the planet with a light "dry haze" (Lamb, 1970) that scatters and reflects sunlight. The resulting reduction of solar radiation to the surface

* Correspondence to: Laboratoire des Sciences du Climat et l'Environnement (LSCE) CNRS, Orme des Merisiers / Bat. 701 C.E. Saclay, 91191 Gifsur-Yvette, France. Tel.: +33 1 69 08 41 58; fax: +33 1 69 08 77 16.
E-mail address: philippe.naveau@lsce.ipsl.fr (P. Naveau).

0167-9473/$ – see front matter © 2012 Elsevier B.V. All rights reserved.
doi:10.1016/j.csda.2012.01.024

can have a strong, albeit short-lived, impact on the climate ranging from several months to a few years (Robock, 2000). Volcanic cooling was found in numerous climate time series, instrumental and proxy alike (Bradley, 1988; Briffa et al., 1998; Crowley, 2000; Jones et al., 2003; Robock and Mao, 1995). Through a large event, or clustering of smaller eruptions, volcanic forcing is thought to be one of the primary factors affecting decadal to century scale evolution of climate (Ammann et al., 2007; Crowley, 2000; Hegerl et al., 2003, 2006). It is therefore important to have a good quantitative estimate of these perturbations through time.

Volcanic forcing histories can be estimated from a host of sources, such as volcanological records (Newhall and Self, 1982; Simkin and Siebert, 1994), instrumental records (Sato et al., 1993; Stothers, 1996a; Ammann et al., 2003), observational information of visible perturbations of atmosphere or the ground (Lamb, 1970), or astronomical observations (Keen, 2001). However, the probably most reliable records that are most consistent in time come from polar ice core series (Gao et al., 2008; Hammer, 1977; Robock and Free, 1995; Zielinski et al., 1994), where volcanic acid or sulfate spikes can be identified within individual snow and ice layers of the generally pristine environments of the ice caps (e.g., see Robock, 2000; Zielinski, 2000, for discussion).

Various techniques have been used to recognize these volcanic deposits, either using electrical conductivity changes to identify the variations in acidity (Hammer, 1977), or more recently through direct measurements of sulfate at very high resolutions throughout the ice cores (Zielinski et al., 1994; Clausen et al., 1997; Palmer et al., 2001; Castellano et al., 2005; Kurbatov et al., 2006). The advantage of using the polar ice sheets as an archive for individual volcanic events is that they preserve the climatically all-important sulfate. If sulfate can be found at multiple locations, then it is highly likely it was transported through the stratosphere, and thus was climatically "active" (Zielinski et al., 1994; Clausen et al., 1997). (In contrast, tropospherically transported sulfate is too short lived in the atmosphere and thus is unlikely to have significant climatic effects.) Deposition can happen both through slow and evenly distributed dry deposition, or through more event-like wet deposition associated with storm systems. The volcanic sulfate signals that can be found at various ice-core locations, therefore, represent a spatial sample of the large-scale deposition. Areas with generally more storm events also commonly exhibit higher sulfate deposition rates. Thus, while each event will likely have some unique weather-related deposition features, there is an underlying spatial pattern that reflects the climatological deposition rates (Mosley-Thompson et al., 1993; Gao et al., 2007). Based on a suite of cores, and thus multiple samples for each event, one can determine what the timing and the flux of sulfate was to the ice sheet, which in turn can be used to estimate the amount of sulfate and thus forcing.

As with all indirect information, using polar ice cores also involves some inherent difficulties. Exact dating of individual ice layers, a pre-requisite for core-to-core comparisons, is more problematic than in biological records, such as tree rings, where time progresses without interruptions. This continuity is not always guaranteed for the small diameter (<15 cm) ice cores because the possibility for stratigraphic disturbance exists. Wind can under some circumstances erase snow layers in such small areas; sometimes it can accumulate more snow, which then forms a false "annual" band. Therefore, the ice coring community has been using characteristic time markers, and in particular a few of the largest volcanic events, as cross-dating hinge-points. Although generally defendable from a physical perspective, this approach could potentially introduce some biases. Exploiting relative time intervals of volcanic signals between these marker events as well as inclusion of other prior knowledge have been corner stones of "expert-based" ice core compilations for volcanic forcing reconstructions (Crowley, 2000; Ammann and Naveau, 2003; Ammann et al., 2007; Gao et al., 2006). A more objective method is desirable. Here we develop the foundation for such a method, but we have to rely on the assumption that the available chronologies are perfectly dated (synchronized), a condition that would have to be assessed in more detail for the full set of existing high-resolution ice core records.

1.2. The statistical problem

Statistically, volcanic perturbations can be viewed as pulse-like events, i.e. short and intense deviations from the climatological (interannual) noise and some underlying longer term variation. The common procedures to identify and then quantify the volcanic signal has been by applying an evolving mean to the individual time series and then selecting signals that pass a certain threshold of noise around this mean (Gao et al., 2008; Robock and Free, 1995). However, classical statistical tools based on averages, variances or projections are not well adapted to capture the true characteristics of the rapid and sharp features of the volcanic eruption and deposition process (Naveau and Ammann, 2005).

Recently, more modern statistical tools using state space models have been used to improve on the identification and quantification process of volcanic events (and thus enhance objectivity) in individual time series (Naveau and Ammann, 2005). Identified events could then be averaged across the different series. While large events were generally easy to recognize, the extraction proved much more difficult for small events that are obscured by the background noise (Naveau et al., 2003). If chronologies of ice cores were synchronized, then modern statistical tools could further exploit the common deposition structure across multiple ice cores, and thus the threshold to recognize events could be lowered significantly. This could make volcanic forcing series more reliable. We build on earlier work (Naveau et al., 2003; Naveau and Ammann, 2005) to develop a statistically sound volcanic extraction process that uses the joint information across a series of ice cores. The geophysical motivation is centered on volcanic sulfate deposits in ice core time series, but techniques developed in this article can equally be used in other applications where large amplitude pulses that are superimposed on slowly changing trends need to be recognized across multiple noisy time series.

One of the difficulties of statistical modeling in the multivariate framework resides in the estimate of a nonlinear and non-Gaussian hidden signal common to all of the time series. For example, in the case of volcanoes, a big eruption will have a strong signal, but the relative magnitude might differ substantially between each of the ice core data sets, and the other components of the series could be quite heterogeneous. From a statistical point of view, a global solution to estimate the parameters is preferable because it reduces the propagation of errors. To solve these problems of extraction, we propose a *multivariate multi-state space model* which integrates the various components (forcing, trends, and noises) in a global mathematical formulation.

We discuss the general concept and properties of our extraction model in Section 2. Then, in Section 3, simulations with a known pulse process embedded in series with different noise characteristics are used to assess the performance of our extraction method. The method is then applied to real ice core data proxies in Section 4. In Section 5, we conclude this article with a brief summary and discussion of the advantages, limitations and possible extensions of our extraction algorithm.

2. Extraction procedure

2.1. State space modeling

State space models have become a practical and powerful tool to model dynamic and complex systems. Closely related to the Kalman filter, they have been used in a wide range of disciplines: biology, economics, engineering, and statistics (see Guo et al., 1999). The fundamental idea of the state space model is that the observed data is linearly dependent on latent variables of interest that vary in time. Mathematically, the observed data are governed by two equations, known as the *observational* and *system equations*. In our case, the observational equation expresses itself as a linear combination of three variables (common forcing, trends, and noise), while the system equations represent the temporal dynamics of the underlying hidden processes. The statistical problem is to deduce the behavior of hidden variables of the pulse-like events from the observed data. Before discussing the aspects of our multivariate approach, we must introduce some notation and clarify our working hypotheses.

2.2. Our model

Suppose we observe J time series over the same time length, say T, and with the same temporal resolution. Each time series is denoted $y_j(t)$. We also assume that each of these time series is affected by a similar pulse-like forcing, say $x(t)$, that is unobserved and has to be estimated. This forcing corresponds to abrupt events and therefore is nonlinear and non-Gaussian. Our first equation explains how the three elements of our statistical model (trends, cycles, pulse-like events and noises) interact

$$y_j(t) = \beta_j\, x(t) + f_j(t) + \epsilon_j(t), \quad \text{for } j = 1, \ldots, J, \text{ and } t = 1, \ldots, T. \tag{1}$$

The hidden, but common, pulse-like signal is represented by the random variable $x(t)$. The scalar β_j can be viewed as a scaling factor that reflects the impact of $x(t)$ on the j-th time series. Note that β_j is site dependent and time invariant. In case of the occurrence of a pulse (i.e. $I_t = 1$), the random variable $v(t)$ is driven by a Gaussian distribution (the Eq. (3) is introduced below). That means that each event has its particular amplitude. This hypothesis represents a simplification of real aerosol load phenomena. The deposition of sulfates on a particular site and originating from a specific volcano may substantially vary from event to event, depending on the atmospheric circulation features, e.g. Wastegard and Davies (2009). The second component $f_j(t)$ corresponds to a smooth trend. The last term, $\epsilon_j(t)$, is simply a background i.i.d. Gaussian random noise process centered about zero with standard deviation σ_j. The different noises in Eq. (1) are assumed to be independent.

The two main differences of our hidden signal $x(t)$ with classical regression models come from its pulse-like nature and its short term memory. To obey this constraint, we construct $x(t)$ as an autoregressive model defined by

$$x(t) = \alpha\, x(t-1) + v(t), \quad \text{for } t = 1, \ldots, T, \tag{2}$$

where $|\alpha| < 1$ is an unknown constant representing the decaying volcanic aerosol removal from the stratosphere and $v(t)$ corresponds to an i.i.d. random sequence and we set $x(0) = 0$. To create a pulse like effect, we impose that the i.i.d. random sequence $v(t)$ follows a mixture of a normal random variables

$$v(t) = \begin{cases} N(\mu_v, \sigma_v^2), & \text{if } I_t = 1, \\ 0, & \text{if } I_t = 0, \end{cases} \tag{3}$$

where $N(\mu_v, \sigma_v^2)$ represents a Gaussian variable with mean μ_v and standard deviation σ_v. In Eq. (3), I_t is a sequence of i.i.d. Bernoulli random variables, whose parameter $\pi = \Pr[I_t = 1]$ denotes the probability of observing a pulse-like event. The random variable $v(t)$ corresponds to the strength associated with a rare event. In contrast, $v(t)$ is set to zero if I_t equals to zero. Eq. (2) allows for a short lived temporal effect of such a forcing. Despite its low number of parameters (π, α, μ_v, β_j, σ_j), the additive model defined by Eq. (1) with this hidden dynamical structure (2) and its pulse-like nature defined by (3) offers enough flexibility to mimic pulse-like events behaviors at an annual scale.

The trends f_j in Eq. (1) are modeled by cubic smoothing splines represented in state space form (Wahba, 1978; Wecker and Ansley, 1983). This representation allows to express a *smooth* function (i.e. a function of which a fixed number m of derivatives are continuous) as a sum of its weighted derivatives and a Wiener process. By choosing $m = 2$ trends $f_j(t)$ can be expressed as functions of its first derivatives,

$$\mathbf{F_j}(t) = B\mathbf{F_j}(t-1) + \mathbf{E}_{f_j}(t),$$

where $\mathbf{F_j}(t) = (f_j(t), f_j^{(1)}(t))$, $B[i,k] = 1/(k-i)!$ for $k \geq i$ or zero otherwise. The two-dimensional vector $\mathbf{E}_{f_j}(t)$ represents a zero mean Gaussian vector with covariance elements $\lambda_j\sigma_j^2/[(i+k-1)(i-1)!(k-1)!]$ where λ_j denotes the smoothing parameter. This spline representation allows to model nonparametric trend, based on series developments similar to Taylor's. The trend is calculated using a polynomial regression and a random residues modeled by a Wiener process (see Abramowitz and Stegun, 1970; Stark and Woods, 2002).

With these notations, it is possible to combine $x(t), f_j(t)$, and their associated noises, and thus to rewrite Eqs. (1)–(3) in matrix form. With the state vector $X_t = (v(t-1), x(t), \mathbf{F_1}(t), \ldots, \mathbf{F_J}(t))^T$ We can define

$$Y_t = HX_t + E_t, \tag{4}$$

where the temporal dynamics is then described by another matrix equation

$$X_t = \Phi X_{t-1} + E_t^*. \tag{5}$$

The matrices H and Φ and the random vectors E_t and E_t^* have explicit (but complex) forms that are given in the Appendix.

A rich literature (Guo et al., 1999; Shepard, 1994) exists to estimate parameters of the state space models. Such techniques are closely related to statistical data assimilation schemes. In Gaussian state space models, the Kalman filter provides an optimal recursive estimate of $x(t)$ from observations $Y_t = (y_1(t), \ldots, y_J(t))$. Unfortunately, the nature of the pulse-like events (the mixture of distribution) implies that the overall assumption of normality is not satisfied (see Eq. (3)). To solve this problem, we drew inspiration from original work of Guo et al. (1999) who offered a variation of the Kalman filter. The principal idea is to approximate the distribution of the mixture of normals by a normal distribution whose first two moments are identical to that of the mixture. The details of this technique within the univariate framework can also be found in Naveau et al. (2003). When the last evaluations of this modified Kalman filter are found, then a sequential backward algorithm is applied (Guo et al., 1999).

3. A simulation study

We show in Fig. 1 three simulated times series, each with a different trend, a background variation of local noise and the common pulse-like signal with its site specific scale (the simulation series were made with $\mu_v = 3.5$, $\sigma_v = 2.63$, $\alpha = 0.7$, and $\pi = 0.3$, as parameters of Eqs. (2) and (3)). The included pulse-process is shown in the two bottom panels of Fig. 1. In the top panel of Fig. 1, the time series $y_1(t)$ combines a discernible cycle (a sinusoidal trend with a constant level shift defined by $f_1(t) = 10 + 15\sin(2\pi((t-1)/90))$) with noise and the pulse-like forcing. In this data set, most pulse-like events are visually identifiable because the noise level is low compared to the pulse amplitude. The middle panel shows a more noisy time series $y_2(t)$ with a linear trend ($f_2(t) = 0.5t$). Here, finding pulse-like events represents already a more difficult challenge. For instance, the small pulses at the beginning of this time series (see bottom panels of Fig. 1), clearly visible in $y_1(t)$, are not easily distinguishable in time series $y_2(t)$. Although the series in the bottom panel of Fig. 1 contains no trend ($f_3(t) = 0$), this series $y_3(t)$ is characterized by the lowest multiplicative factor ($\beta_3 = 7.5$) for the pulse-like events among the three simulated time series, i.e. the common underlying signal in $y_3(t)$ is less apparent in the large noise.

Fig. 2 shows the results in the multivariate case (top panel) as well as for each of the three individual series if they would be treated separately. Each panel compares the identified events (solid line) with the timing of the true events that were embedded as hidden pulses in all three series (gray bars). Overall, the multivariate model was effective in identifying the hidden pulses and the joint extraction is capable of highlighting features that were not detected by the individual analyses, e.g. the double peak just before $t = 400$.

The increasing noise in series $y_2(t)$, and particularly $y_3(t)$, obviously impacts the extraction process. The shortcomings express themselves both in the less accurate identification (less) of the imposed events as well as in the rather volatile event magnitude.

This is illustrated through a scatter plot (Fig. 3) for each identified event, where the magnitude of the true (hidden) process (x) is compared against the estimates ($\hat{x}$). The graph highlights that the multivariate algorithm is able to estimate most accurately (up to a multiplicative constant) the amplitudes of the hidden pulses. Also the extraction from the low-noise series $y_1(t)$ was successful and contains most of the events. The overall estimate of the amplitude across all cases is more accurate in the multi-variate case, despite two rather unfavorable additional series $y_2(t)$ and $y_3(t)$.

The extraction procedure not only quantifies the pulse-like events but also offers the full information about the underlying trends. Fig. 4 shows that the three trends f_j of Eq. (1) are well captured.

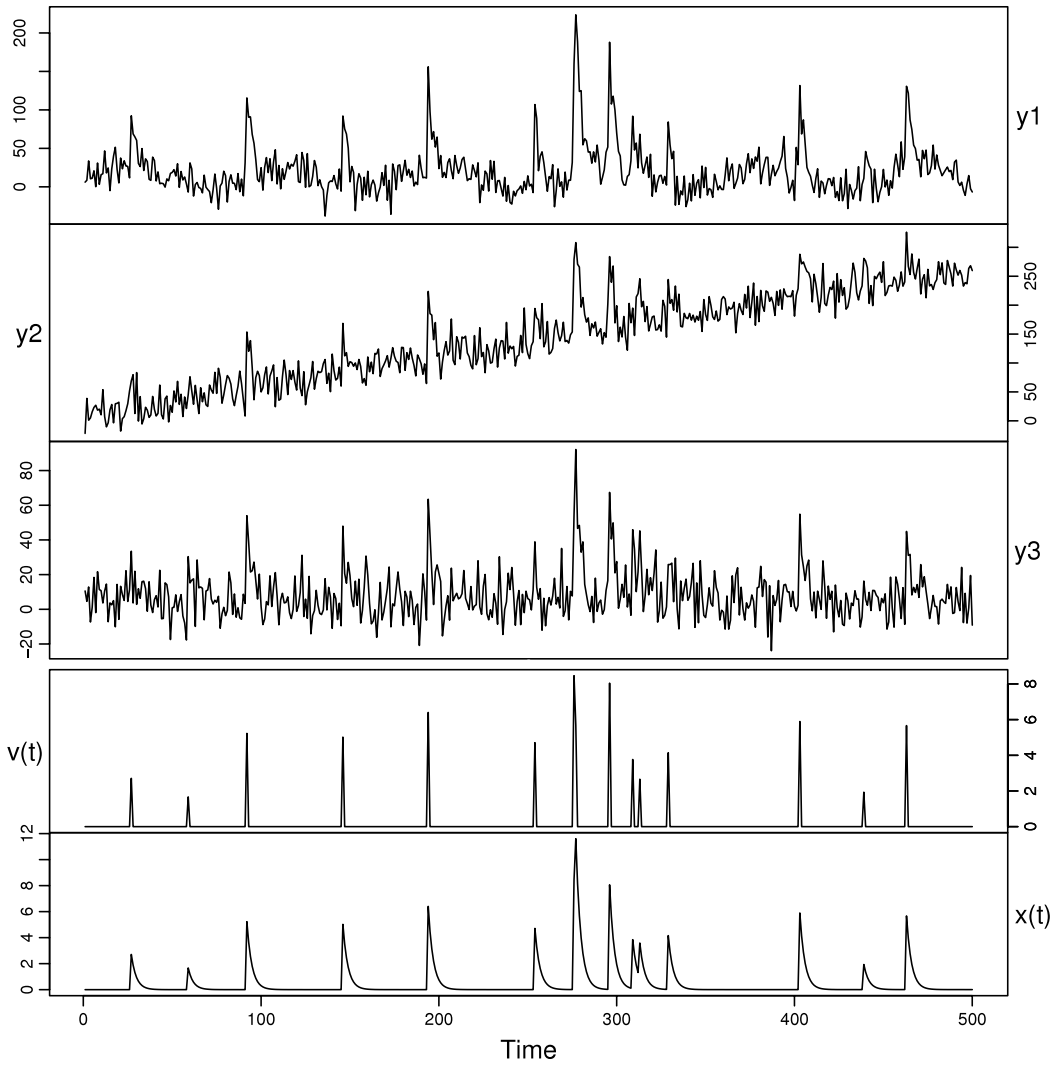

Fig. 1. Simulated data from Eq. (1) with $J = 3$. All series represent samples over a time span of 500 years and were simulated with the following parameter setting: the standard deviations observation noises: $(\sigma_1, \sigma_2, \sigma_3) = (15, 20, 10)$, the parameters of pulse amplitudes: $(\beta_1, \beta_2, \beta_3) = (20, 15, 7.5)$, the pulse occurrence probability: $\pi = 0.03$, the Auto-Regression parameter of x : $\alpha = 0.7$, the common mean pulse amplitude of v: $\mu_v = 3.5$, the standard deviation of pulse event amplitude: $\sigma_v = 2.63$. The two bottom panels represent the simulated pulse-like time series hidden in the three time series obtained from Eqs. (2) and (3) with $\mu_v = 3.5$, $\sigma_v = 2.63$ and $\pi = 0.03$.

4. Application to ice core data

In the real world, the most reliable records of volcanic pulses come from ice cores. The idealized experiment shown above does not represent the true levels of noise and core-to-core differences in the deposition. Therefore, to test our method with realistic data, we now apply the multi-variate extraction to five selected series from Greenland covering the period from 1645 to 1980 at annual resolution. As indicated above by the simulation results, doing a multivariate extraction rather than separate individual analysis that subsequently gets averaged has benefits for both recognizing particularly small events against the varying noise of different cores, and estimate more reliably the amplitude of volcanic pulses across Greenland where individual cores have substantially different absolute signals. Because we apply a joint-signal extraction through the multi-variate state-space model, we obtain a unitless, joint volcanic pulse history that is based on the mean contributions from individual ice cores. This unitless series can then be calibrated against known (i.e. measured) volcanic deposition or forcing, a substantial improvement over previous methods where individual records had to be calibrated based on a few noisy events, and to obtain an overall series, these noisy estimates had to be averaged.

Fig. 5 shows five ice core records from Greenland with the identified trends from the multi-variate extraction procedure. Differences in series, their trends as well as the variance of the sulfate deposition are roughly representative for the full set of polar ice cores.

Table 1 and Fig. 6 show the extracted pulses (top panel) and their associated posterior probabilities (middle panel) resulting from the multi-variate state-space model. Five high-probability, about three intermediate-probability and several low-probability events are recognized across the series. While large events are often identified with high confidence, applying the extraction procedure to individual ice cores would include more, but often erroneous spikes in the list. The

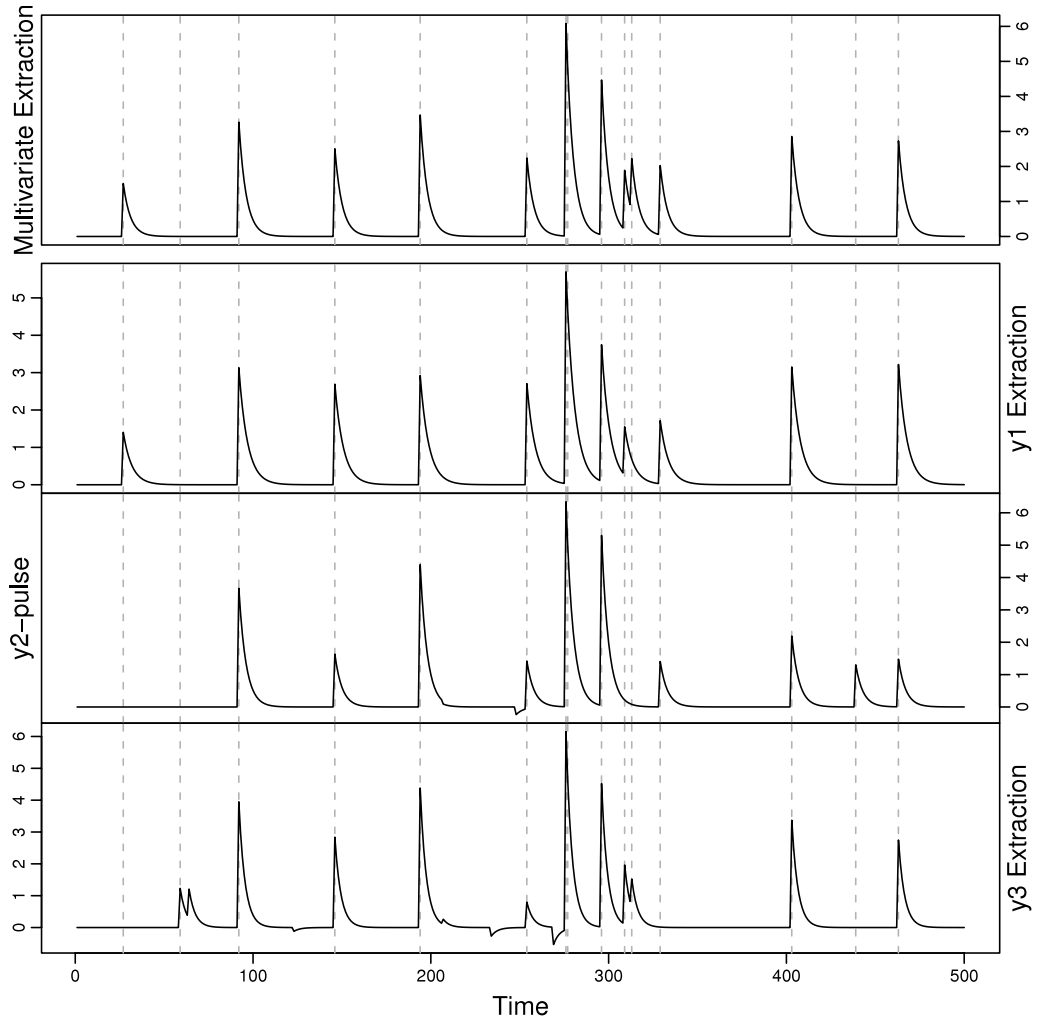

Fig. 2. Estimated pulse-like amplitudes. The top panel corresponds to the *multivariate* extraction and the other three panels represent the *univariate* extraction applied to individually to each time series from Fig. 1, respectively y_1, y_2 and y_3. Note that the multivariate extraction dismissed the "negative" spurious events detected on the 2nd and 3rd series. Note also that the multivariate extraction allows to detect more actual pulse like events than the different univariate cases.

bottom panel of Fig. 6 illustrates this fact with the extracted signal on the first of the ice core series. A whole series of "high-probability" events are "found" throughout the 20th century. These spikes, however, do not have any counterparts in the other series, and thus, despite the fact that they are large and recognized with high confidence in the individual record of series one, the *joint* likelihood is much lower. At the same time, more of the small volcanic inputs are recognized in the joint extraction with higher confidence, a capability that cannot be achieved at the individual level where small events tend to get overwhelmed by the background noise. The joint extraction reduces the noise and therefore is more sensitive towards small events.

Looking at the magnitude of events, one particular deposition event in the year 1783 is immediately recognizable across the five series. It is the result of the well documented, large and intensive Laki eruption sequence in Iceland (Thordarson and Self, 2003). This eruption quite likely did lead to a substantial non-stratospheric transport of sulfate towards nearby Greenland, causing the exceptional volcanic signal. Therefore, compared to low-latitude events whose sulfate aerosol get spread in the stratosphere across both hemispheres, this eruption appears disproportionally large, despite the fact that its regional effects were tremendous (Stothers, 1996b).

In contrast, the famous tropical eruption of Tambora of 1815 was recognized by the extraction with a signal less than one third of the 1783 Laki deposit, but nevertheless it was identified with high confidence (high posterior probability). Given the global spread of its aerosol, and no chance for any tropospheric transport of the sulfate, the stratospheric mass loading of Tambora must have been very large. Yet, it has to be calibrated differently than the Laki signal to obtain a global stratospheric mass. This difference between quasi-local high-latitude events and tropical eruptions represents one of the difficulties in the interpretation of polar-based ice core records of volcanic forcing. While corrections can easily be applied for these well-known events, lesser known, or even unknown, eruptions require more detailed analyses, such as the evaluation of other, the timing and deposition of other chemical species that could indicate local transport (Clausen et al., 1997), or synchronous deposition in Antarctica and Greenland which would point to a tropical source (Palais et al., 1992; Langway et al., 1995; Ammann and Naveau, 2003). But particularly for small events, this distinction is very difficult (Crowley, 2000).

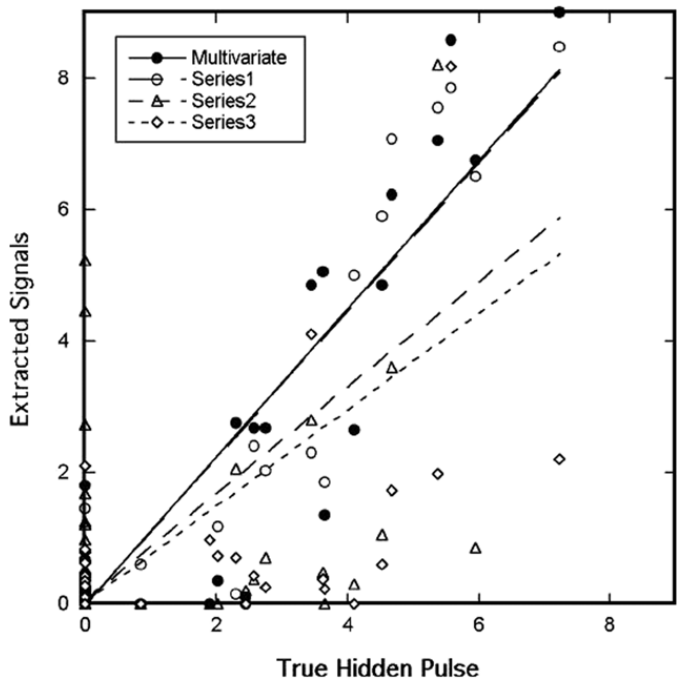

Fig. 3. The x-axis represents the standardized hidden $x(t)$ and the y-axis corresponds to our estimated standardized $\hat{x}_t$ from the data displayed in Fig. 1. Black circles corresponding to the multivariate extraction better estimate amplitudes of the pulse like events than the different univariate cases.

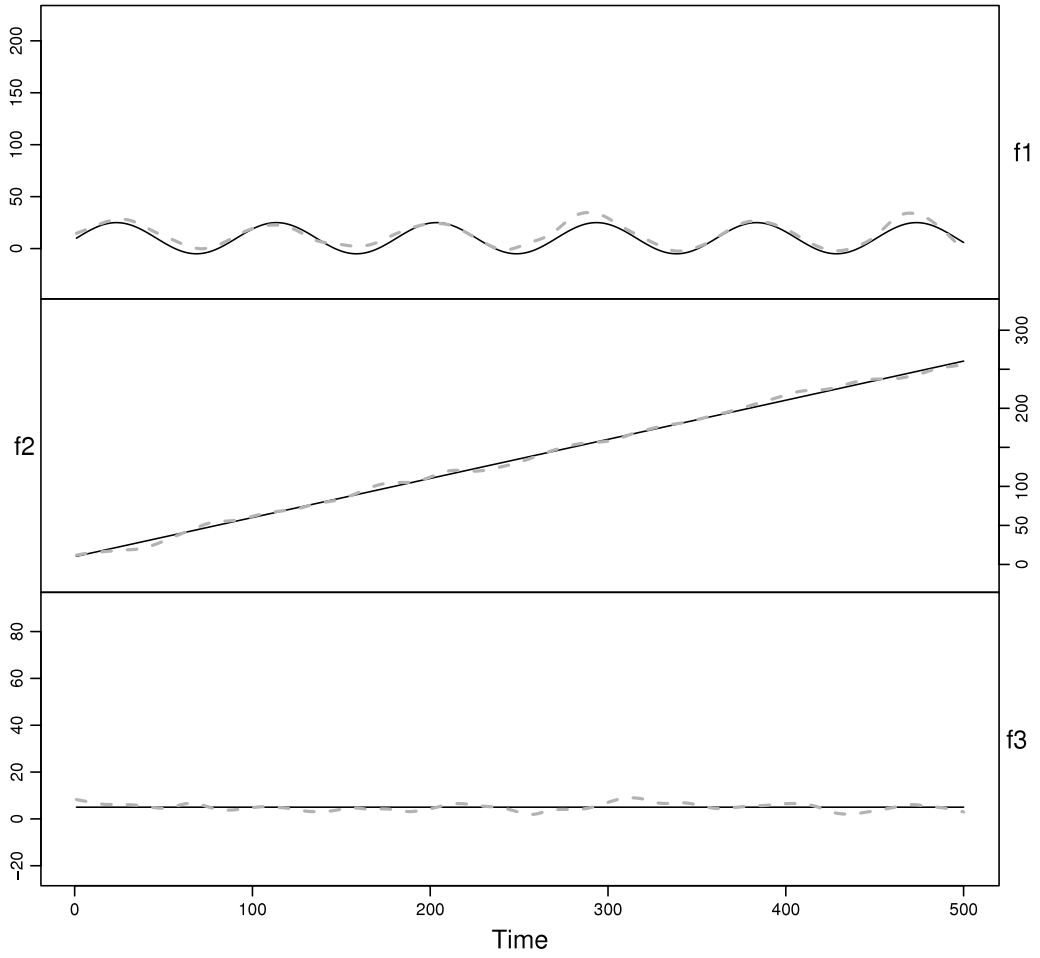

Fig. 4. The solid black curves represent the hidden trend f_j and the dotted lines correspond to our estimated trend $\hat{f}_j$ for each of the time series displayed in Fig. 1.

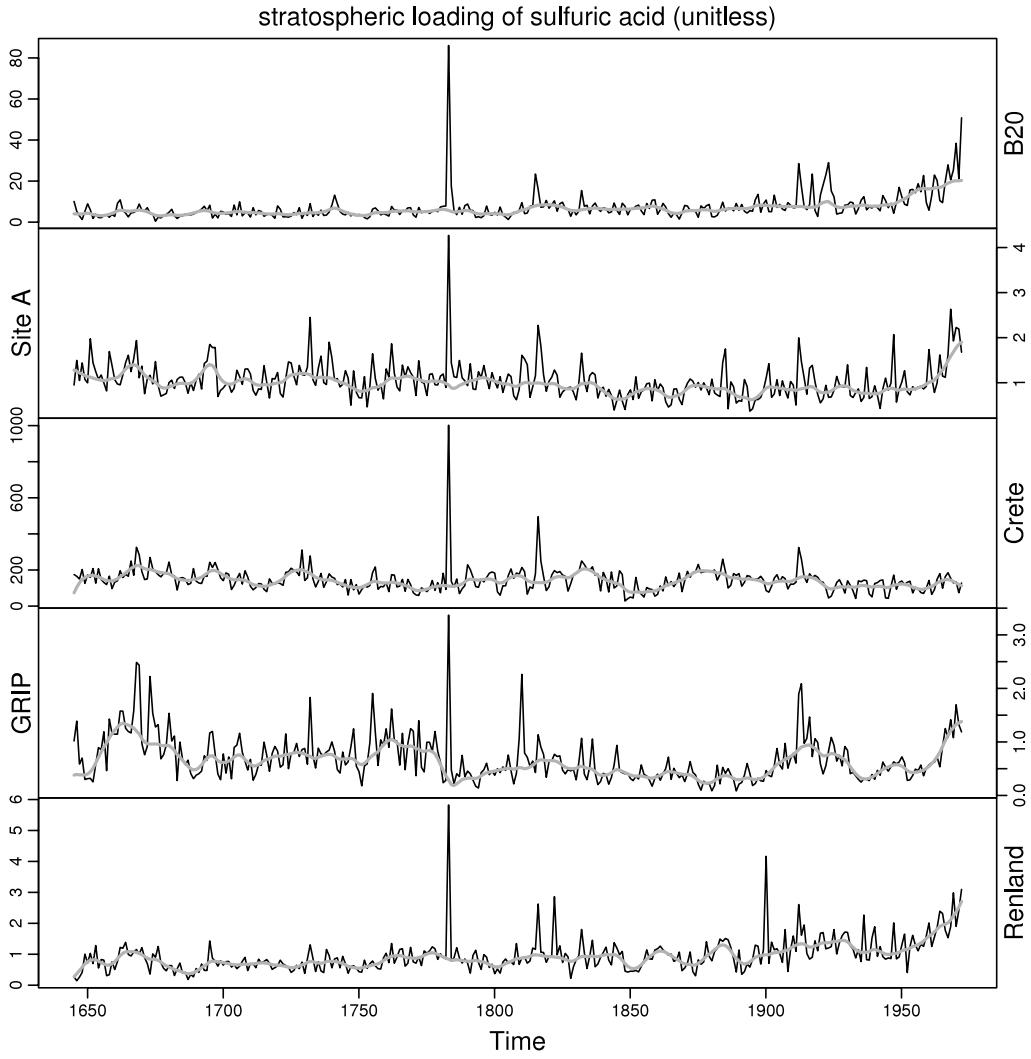

Fig. 5. Five unitless volcanic history ice core records of sulfate deposits from Greenland covering the period from 1645 to 1980 at annual resolution, with the estimated trends obtained from our multivariate extraction (gray lines).

The fifteen events listed in Table 1 contain some well-known events as well as some clearly unknown signals. We list the likely source volcanoes, but should not forget to consult the posterior-probability to evaluate if these events are to be regarded as robust.

To convert the volcanic pulse history into an estimate of a forcing, the amplitudes of the unitless ice core-extracted volcanic pulses need to be scaled to units such as "stratospheric loading of sulfuric acid" (Gao et al., 2008; Zielinski et al., 1994) or radiative forcing (Hansen and Coauthors, 2002; Wigley et al., 2005). The individual ice cores series do not contain local volcanic pulse signals that are directly comparable because of spatial differences in volcanic sulfate deposition (Gao et al., 2007). Therefore, the output from the extraction procedure actually provides only the relative magnitudes of events. This series needs to be *calibrated* against other information, such as the conversion of the mean sulfate fluxes at a particular site to the stratospheric loading over a known period or by simply using a reference event (e.g. Pinatubo or El Chichon) (see Gao et al., 2008, for discussion).

As discussed for the simulated cases above, real world records exhibit often a combination of variations coming from an evolving trend and background noise in addition to the volcanic pulses. Some of these variations can be simple noise, others could potentially be interesting climatically. However, particularly with regard to sulfate deposition, real world records sometimes suffer from a distinct, fundamental change over the last century as human fossil fuel burning has artificially released large amounts of sulfur into the atmosphere. Thus, most Northern Hemisphere records exhibit a systematic increase in the background deposition (Mayewski et al., 1986; Neftel et al., 1985). Sulfate records from the 20th century should therefore be analyzed and interpreted with caution. Looking at individual records (Figs. 5 and 6), a clear increase in the background noise as well as in the variance can be seen. The danger of erroneously identifying some of these anomalies as volcanic spikes exists in the individual extraction (Fig. 6(b)), but the joint extraction is clearly less sensitive to this. Nevertheless, all of 20th century signals should be interpreted with caution.

In summary, compared to individual extraction of volcanic signal for each series, the joint extraction offers a more robust identification of events against noise, and the sensitivity for capturing small eruptions is increased. This benefit is already

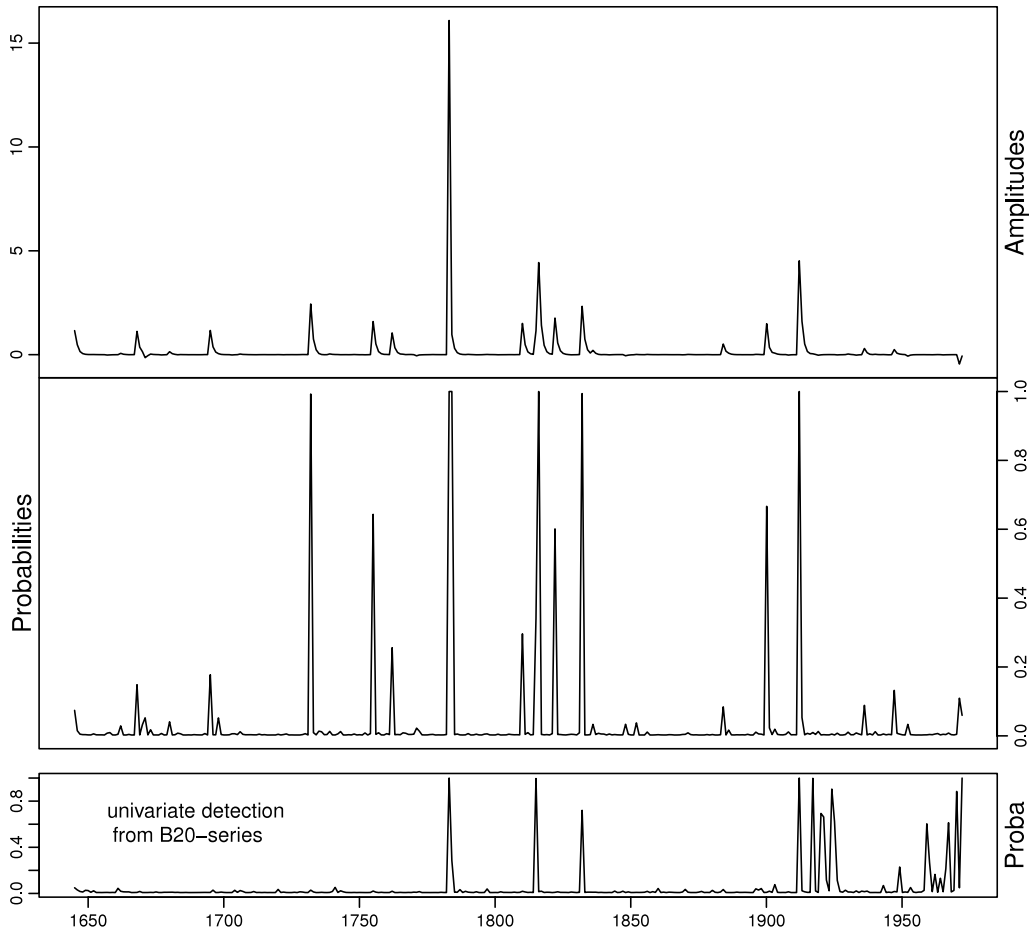

Fig. 6. Estimated magnitudes and associated event probabilities extracted from the five ice cores using the multivariate extraction approach. The bottom panel illustrates the erroneous spikes extracted using a univariate procedure throughout the 20th century.

Table 1
Parallel between the detected events from our method (see Fig. 6) and date of known volcanoes found in the literature (e.g. Wastegard and Davies, 2009). Note that 20th century records quite likely only show Katmai–Novarupta, while others, after 1912, are considered as spurious due to anthropogenic noise. The second column gives the relative amplitudes comparatively to the biggest event (i.e. the Laki eruption in 1783). The five last columns show whether or not the pulse like signal was detected using a univariate procedure on each time series.

Year	Ampl	Proba	Poss. Volcano	y1	y2	y3	y4	y5
1668	0.070	0.35	Shikotsu				*	
1695	0.073	0.24	Komagatake?Serua?Hekla?					
1732	0.152	0.91	Unknown (Lanzarote?)		*		*	
1755	0.099	0.64	Taal? or Katla?				*	
1762	0.065	0.26	Unknown					
1783	**1.00**	**1.00**	Laki (Grimsvoetn)	*	*	*	*	*
1810	0.093	0.35	Unknown tropical				*	
1815	0.071	0.65	Tambora	*		*		*
1822	0.109	0.60	Galunggung					*
1832	0.145	0.95	Babuyan Claro?	*				
1884	0.032	0.11	Krakatau					
1900	0.093	0.66	Unknown					*
1912	0.281	0.98	Katmai–Novarupta	*	*	*	*	*

recognizable in this small sample of five ice core records from Greenland. In a future study, we will apply this technique to the full set of volcanic series from both Greenland and Antarctica to establish a new volcanic sulfate history that can be added to the currently existing series of Crowley and Kim (1999), Ammann et al. (2007), Gao et al. (2008) and Wastegard and Davies (2009).

Before discussing this work, we want to add a few comments about the fitting of the model with the actual series. The first question underlying this application is about the use of a Gaussian distribution in Eq. (3). The choice of Gaussian distribution could implies the occurrence of "negative" volcanic events. This could happen when the mean μ_v of $v(t)$ is small with respect to the variance σ_v. In the simulation shown in Fig. 1 we choose μ_v large enough to avoid that to happen. In the application, the parameter μ_v appears to be large enough with respect to σ_v.

Another related comment is needed. Volcanic eruptions are sometimes assumed to be driven by lognormal distribution instead of Gaussian (e.g. Castellano et al., 2004). To test this assumption, we run our model on the log transformation of the signal $y_j(t) : \log(y_j(t))$. This transformation allows roughly to change the supposed log-normal distribution of the amplitudes of the events into a normal distribution. Results of this study show the same detected events as when running the model directly on $y_j(t)$. Nevertheless, this logarithmic transformation is not satisfactory because it does not allow to separate the different components of the additive equation (1), which is the main goal of the current study. Fig. 6 showing the estimated pulses and the parallel with Table 1, with regards to previous work on volcanic eruptions show that the detected eruptions are relevant with history. These results mean that the assumption that volcanic amplitudes distribution can be approximated by a Gaussian distribution can be considered as relevant for this specific example.

5. Discussion

In this article, we introduced a state space model which allows for the extraction of timing and amplitude of pulse-like events in the presence of trends and noise. The algorithm developed here is applied to multivariate time series with a common hidden forcing. Beyond the problem of detection of the impact of volcanic eruptions on temperature time series, we believe that this type of statistical procedure is flexible enough to be able to work equally well with other time series consisting of large amplitude pulses superimposed on slowly changing trends as may be found in hydrology.

It is possible, or even desirable, to further extend this type of extraction model. In paleoclimatology, it is very rare to have perfect chronologies. Additionally, the time resolution (temporal sampling) can vary across the multitude of different types of records and time series that cover the period of interest. For instance, ice-core chronologies that were established by counting visible/detectable annual layers might be get off-track through missing or repeated layers through wind action. This potential "drift" in chronologies needs to be corrected. For the purpose of a cleaner introduction of our method, we have not dealt with this issue. But before the method can be applied to the full set of ice core records, clearly, their chronologies need to be synchronized. Clustering and other techniques could make this process significantly more objective and reproducible. We are currently exploring such methods. Further, we are adapting our algorithm so that it could deal with non-regular time steps and thus could combine low-resolution (say annual) with high-resolution (full seasonal resolution) data without having to average time series ahead of time. Finally, we are re-evaluating the assumption that the unpredictable noise ϵ_j in (1) are no longer i.i.d., but have a spatial structure in their covariance. These next efforts illustrate that different degrees of complexity can be added to our current model. The challenge for the geophysicist is to ensure that all information is used properly, while the challenge for the statistician is to keep the extended model simple enough for easy interpretation, and for the procedure to be able to actually estimate the necessary parameters. Overall, such collaborations between statisticians and geoscientists have the potential of advancing (in this case climate) research (Hughes and Ammann, 2009) by improving the quantitative treatment of the diverse records and by introducing a formal way of handling uncertainties.

Acknowledgments

This work was supported by the NSF-CMG (ATM-0327936) grant, the NCAR Weather and Climate Impact Assessment Science Initiative, the EU-FP7 "AACQWA" Project (www.acqwa.ch) under contract No. 212250, the PEPER-GIS project, the ANR-MOPERA project and the GEOmon project (www.geomon.eu). The authors would also like to credit the contributors of the R project. The National Center for Atmospheric Research is sponsored by the National Science Foundation.

Appendix

A.1. General remarks and notations about the estimation procedure

To identify and interpret the parameters β_j in (1), we have to force the variance of $x(t)$ to be equal to one. This constraint imposes that σ_v and μ_v has to obey the relationship $1-\alpha^2 = \sigma_v^2\ \pi + \mu_v^2\ \pi\ (1-\pi)$, because of (2) and (3). This implies $\sigma_v^2 = \frac{1}{\pi}(1-\alpha^2-\mu_v^2\ \pi\ (1-\pi))$.

The matrices H and Φ and the random vectors E_t and E_t^* in Eqs. (4) and (5) are defined in as follows

$$H = \begin{bmatrix} 0 & \beta_1 & 1 & 0 & 0 & 0 & 0 & 0 & 0 & 0 & 0 & 0 \\ 0 & \beta_2 & 0 & 0 & 1 & 0 & 0 & 0 & 0 & 0 & 0 & 0 \\ & \vdots & & & & & & & & & & \\ 0 & \beta_J & 0 & 0 & 0 & 0 & 0 & 0 & 0 & 0 & 1 & 0 \end{bmatrix},$$

and

$$\Phi = \begin{bmatrix} 0 & 0 & 0 & 0 & 0 & 0 \\ 1 & \alpha & 0 & 0 & 0 & 0 \\ 0 & 0 & B_1 & 0 & 0 & 0 \\ & & & & \ddots & \\ 0 & 0 & 0 & 0 & 0 & 0 \\ 0 & 0 & 0 & 0 & 0 & B_J \end{bmatrix}, \quad \text{with } B_j = \begin{bmatrix} 1 & 1 \\ 0 & 1 \end{bmatrix},$$

with $E_t = (\epsilon_1, \epsilon_2, \ldots, \epsilon_J)^T$ and $E_t^* = (0, 0, E_{f_1}^T(t), \ldots, E_{f_J}^T(t))^T$, where $E_{f_j}(t)$ follows a zero-mean bivariate normal distribution with covariance $\lambda_j \sigma_j^2 \begin{bmatrix} 1 & \frac{1}{2} \\ \frac{1}{2} & \frac{1}{3} \end{bmatrix}$. Here H corresponds to a $J \times [2(J+1)]$-matrix, E to a J-vector, Φ to a $[2(J+1)] \times [2(J+1)]$-matrix and E^* to a $2(J+1)$-vector.

The estimation of the parameters is accomplished by sequential updating the system and observational equations in a similar manner as presented in appendices (Guo et al., 1999; Naveau et al., 2003). However, there are slight differences since this algorithm is extended to a multivariate framework. See details below in Appendix A.2.

Although the smoothing parameter can be chosen using an automatic method through cross validation techniques, λ_j remains a free choice by the user in our algorithm. From experience, we find that a small value of λ_j such as 0.01 works well with our simulated and real data sets. Using the same value of λ_j across all data sets aided in the comparison of the results.

A.2. Multivariate MKF

For any given values of the parameters of interest, the first step of this multivariate extension of the multiprocess Kalman Filter begins with an initial estimate of $\hat{X}(t-1|Y_{t-1})$ (resp. $\hat{\Sigma}(t-1|Y_{t-1})$) which are defined as the expectation of X_{t-1} conditioned on the observations $Y_{t-1} = (y_1, \ldots, y_{t-1})$ (resp. the variance of X_{t-1} conditioned on the observations Y_{t-1}). The estimation of the parameters is carried out by performing the following steps.

1. Conditioned on $Z_{t-1,i} = (Y_{t-1}, I_t = i)$, the distribution of $\hat{X}_t$ is characterized by the first two moments:

$$\begin{aligned} \hat{X}(t|Z_{t-1,i}) &= \mathbb{E}[X_t|Z_{t-1,i}], \\ &= \Phi \hat{X}(t-1|Y_{t-1}) + \mathbb{E}E[E_j(t|I_t = i)], \end{aligned}$$

and

$$\begin{aligned} \hat{\Sigma}(t|Z_{t-1,i}) &= \mathbb{V}\mathrm{ar}[X_t|Z_{t-1,i}] \\ &= \Phi \hat{\Sigma}(t-1|Y_{t-1})\Phi^T + \mathrm{Cov}[E_j(t|I_t = i)], \\ \mathbb{E}[E_j(t|I_t = i)] &= (\mu_v(t), \mu_v(t), 0, \ldots, 0)^T, \quad \text{if } i = 1, \\ &= (0, 0, 0, \ldots, 0)^T, \quad \text{else.} \end{aligned}$$

$$\mathrm{Cov}[E_j(t|I_t = i)] = \begin{bmatrix} \Sigma_v & 0 & 0 & 0 \\ 0 & \mathrm{Cov}(E_{f_1}(t)) & 0 & 0 \\ & & \ddots & \\ 0 & 0 & & 0 \\ 0 & 0 & 0 & \mathrm{Cov}(E_{f_J}(t)) \end{bmatrix},$$

$$\Sigma_v = \begin{bmatrix} \sigma_v^2 & \sigma_v^2 \\ \sigma_v^2 & \sigma_v^2 \end{bmatrix}.$$

Recall that $\mathbf{E}_{f_j}(t)$ is a 2-dimensional vector with zero mean and covariance elements $\lambda_j \sigma_j^2 / [(i+k-1)(i-1)!(k-1)!]$.

2. The predicted distribution of $Y_t = (y_1(t), y_2(t), \ldots, y_J(t))^T$ conditioned on $Z_{t-1,i}$ is also characterized by the first two moments:

$$\begin{aligned} \mathbb{E}[Y_t|Z_{t-1,i}] &= H\hat{X}(t|Z_{t-1,i}), \\ \mathbb{V}\mathrm{ar}[Y_t|Z_{t-1,i}] &= H\hat{\Sigma}(t|Z_{t-1,i})H^T + \mathbb{V}\mathrm{ar}(\epsilon), \end{aligned}$$

where

$$\mathbb{V}\mathrm{ar}(\epsilon) = \begin{bmatrix} \sigma_1^2 & 0 & 0 & 0 \\ 0 & 0 & \ddots & 0 \\ 0 & 0 & 0 & \sigma_J^2 \end{bmatrix}.$$

The distribution of $(Y_t|Y_{t-1})$ is a mixture of multivariate normal distributions ($\mathcal{MVN}$):

$$(1-\pi)\mathcal{MVN}(\mathbb{E}[Y_t|Z_{t-1,0}], \mathbb{V}\mathrm{ar}[Y_t|Z_{t-1,0}]) + \pi\mathcal{MVN}(\mathbb{E}[Y_t|Z_{t-1,1}], \mathbb{V}\mathrm{ar}[Y_t|Z_{t-1,1}]).$$

3. The posterior probability of index variable $I_t = i$ conditioned on Y_t is then given by

$$\Pr(I_t = 0|Y_t) = \frac{(1-\pi)\mathcal{MVN}(\mathbb{E}[Y_t|Z_{t-1,0}], \mathbb{V}\mathrm{ar}[Y_t|Z_{t-1,0}])}{\Pr(Y_t|Y_{t-1})},$$

and

$$\Pr(I_t = 1|Y_t) = \frac{\pi\mathcal{MVN}(\mathbb{E}[Y_t|Z_{t-1,1}], \mathbb{V}\mathrm{ar}[Y_t|Z_{t-1,1}])}{\Pr(Y_t|Y_{t-1})}.$$

4. Given Y_t we can update the first two moments of X_t conditioned on I_t:

$$\hat{X}(t|Y_t, I_t = i) = \hat{X}(t|Z_{t-1,i}) + \hat{\Sigma}(t|Z_{t-1,i})H^T[\mathbb{V}\mathrm{ar}(Y_t|Z_{t-1,i})]^{-1}[Y_t - Y(t|Z_{t-1,i})],$$

and

$$\hat{\Sigma}(t|Z_t) = \hat{\Sigma}(t|Z_{t-1,i}) - \hat{\Sigma}(t|Z_{t-1,i})H^T\mathbb{V}\mathrm{ar}[Y_t|Z_{t-1,i}]^{-1}H\hat{\Sigma}(t|Z_{t-1,i}).$$

5. Marginal distribution of $\hat{X}(t|Y_t)$ is a mixture of multivariate normals. We approximate the mixture by a multivariate normal with the same first two moments.

$$\hat{X}(t|Y_t) = (1-\pi)\hat{X}(t|Z_{t,0}) + \pi\hat{X}(t|Z_{t,1}),$$

and

$$\hat{\Sigma}(t|Y_t) = (1-\pi)\hat{\Sigma}(t|Z_{t,0}) + \pi\hat{\Sigma}(t|Z_{t,1}) + (\hat{X}(t|Z_{t,i}) - \hat{X}(t|Y_t))(\hat{X}(t|Z_{t,i}) - \hat{X}(t|Y_t))^T.$$

This steps allows us to continue sequential updating.

References

Abramowitz, M., Stegun, I.A., 1970. Handbook of Mathematical Functions: With Formulas, Graphs, and Mathematical Tables.

Ammann, C., Joos, F., Schimel, D., Otto-Bliesner, B., Tomas, R., 2007. Solar influence on climate during the past millennium: results from transient simulations with the ncar climate system model. Proceedings of the National Academy of Sciences 104, 3713–3718.

Ammann, C., Meehl, G.A., Washington, W., Zender, C., 2003. A monthly and latitudinally varying volcanic forcing dataset in simulations of 20th century climate. Geophysical Research Letters 30, doi:10.1029/2003GL016875.

Ammann, C., Naveau, P., 2003. Statistical analysis of tropical explosive volcanism occurrences over the last 6 centuries. Geophysical Research Letters 30, doi:10.1029/2002GL016388.

Bradley, R., 1988. The explosive volcanic eruption signal in Northern Hemisphere continental temperature records. Climate Change 12, 221–243.

Briffa, K., Jones, P., Schweingruber, F., Osborn, T., 1998. Influence of volcanic eruptions on Northern Hemisphere summer temperature over the past 600 years. Nature 393, 450–455.

Castellano, E., Becagli, S., Hannson, M., Hutterli, M., Petit, J.R., Rampino, M., Severi, M., Steffensen, J.P., Traversi, R., Udisti, R., 2005. Journal of Geophysical Research 110, doi:10.1029/2004JD005259.

Castellano, E., Becagli, S., Jouzel, J., Migliori, A., Severi, M., Steffensen, J., Traversi, R., Udisti, R., 2004. Global and Planetary Change 42, doi:10.1016/j.gloplacha.2003.11.007.

Clausen, H., Hammer, C., Hvidberg, C., Dahl-Jensen, D., Steffensen, J., Kipfstuhl, J., Legrand, M., 1997. A comparison of volcanic records over the past 4000 years from the Greenland ice core project and dye 3 Greenland ice cores. Journal of Geophysical Research 102.

Crowley, T., 2000. Causes of climate change over the past 1000 years. Science 289, 270–277.

Crowley, T.J., Kim, K.-Y., 1999. Modeling the temperature response to forced climate change over the last six centuries. Geophysical Research Letters 26.

Gao, C., Oman, L., Robock, A., Stenchikov, G., 2007. Atmospheric volcanic loading derived from bipolar ice cores: accounting for the spatial distribution of volcanic deposition. Journal of Geophysical Research 112, doi:10.1029/2006JD007461.

Gao, C., Robock, A., Ammann, C., 2008. Volcanic forcing of climate over the past 1500 years: an improved ice-core based index for climate models. Journal of Geophysical Research.

Gao, C., Robock, A., Self, S., Witter, J.B., Steffenson, J., Clausen, H.B., Siggaard-Andersen, M., Johnsen, S., Mayewski, P.A., Ammann, C., 2006. The 1452 or 1453 A.D. Kuwae eruption signal derived from multiple ice core records: greatest volcanic sulfate event of the past 700 years. Journal of Geophysical Research 111, doi:10.1029/2005JD006710.

Guo, W., Wang, Y., Brown, M., 1999. A signal extraction approach to modeling hormone time series with pulses and a changing baseline. Journal of the American Statistical Association 94, 746–756.

Hammer, C., 1977. Past volcanism revealed by Greenland Ice Sheet impurities. Nature 270, 482–486.

Hansen, J., Coauthors, 2002. Climate forcings in goddard institute for space studies si2000 simulations. Journal of Geophysical Research (Atmospheres) 107.

Hegerl, G., Crowley, T., Baum, S., Kim, K., Hyde, W., 2003. Detection of volcanic, solar and greenhouse gas signals in paleo-reconstructions of Nothern Hemispheric temperature. Geophysical Research Letters 30 (5), 1242. doi:10.1029/2002GL016271.

Hegerl, G., Crowley, T., Hyde, W., Frame, D., 2006. Climate sensitivity constrained by temperature reconstructions over the past seven centuries. Nature 440, 1029–1032. doi:10.1038/nature04679.

Hughes, M.K., Ammann, C.M., 2009. The future of the past—an earth system framework for high resolution paleoclimatology: editorial essay. Climatic Change 94, doi:10.1007/s10584-009-9588-0.

Jones, P., Moberg, A., Osborn, T., Briffa, K., 2003. Surface climate responses to explosive volcanic eruptions seen in long European temperature records and mid-to-high latitude tree-ring density around the Northern Hemisphere. In: Robock, A., Oppenheimer, C. (Eds.), Volcanism and the Earth's Atmosphere. In: Geophysical Monograph, (ISSN: 0065-8448), vol. 139. pp. 239–254. doi:10.1029/139GM15.

Keen, R., 2001. Volcanic aerosol optical thicknesses since 1960. Global Volcanism Network 26.

Kurbatov, A.V., Zelinski, G.A., Dunbar, N.W., Mayewski, P.A., Meyerson, E.A., Sneed, S.B., Taylor, K.C., 2006. A 12,000 year record of explosive volcanism in the siple dome ice core, West Antarctica. Journal of Geophysical Research 111, doi:10.1029/2005JD006072.

Lamb, H., 1970. Volcanic dust in the atmosphere: with a chronology and assessment of its meteorological significance. Philosophical Transactions of the Royal Society of London Series A 266, 425–533.

Langway, C.J., Osada, K., Clausen, H., Hammer, C.U., Shoji, H., 1995. A 10-century comparison of prominent bipolar volcanic events in ice cores. Journal of Geophysical Research 100.

Mayewski, P., Lyons, W., Spencer, M., Twickler, M., Koci, P., Dansgaard, P., Davidson, C., Honrath, R., 1986. Sulfate and nitrate concentrations from a South Greenland ice core. Science 232, 975–977.

Mosley-Thompson, E., Thompson, L., Dai, J., Davis, M., Lin, P., 1993. Climate of the last 500 years: high resolution ice core records. Quaternary Science Reviews 12.

Naveau, P., Ammann, C., 2005. Statistical distributions of ice core sulfate from climatically relevant volcanic eruptions. Geophysical Research Letters 32, doi:10.1029/2004GL021732.

Naveau, P., Ammann, C., Oh, H., Guo, W., 2003. An automatic statistical methodology to extract pulse like forcing factors in climatic time series: application to volcanic events. Geophysical Monograph (ISSN: 0065-8448) 139, 177–186.

Neftel, A., Beer, J., Oeschger, H., Zürcher, F., Finkel, R., 1985. Sulphate and nitrate concentrations in snow from South Greenland 1895–1978. Nature 314, 611–613.

Newhall, C., Self, S., 1982. The volcanic explosivity indes (VEI): an estimate of explosive magnitude for historical volcanism. Journal of Geophysical Research 87, 1231–1238.

Palais, J., Germani, M., Zielinski, G., 1992. Interhemispheric transport of volcanic ash from a 1259 ad volcanic-eruption to the Greenland and Antarctic ice sheets. Geophysical Research Letters 19.
Palmer, A.S., van Ommen, T.D., Curran, M.A.J., Morgan, V., Souney, J.M., Mayewski, P.A., 2001. High-precision dating of volcanic events (A.D. 1301–1995) using ice cores from law dome, Antarctica. Journal of Geophysical Research 106.
Robock, A., 2000. Volcanic eruptions and climate. Reviews of Geophysics 38, 191–219.
Robock, A., Free, M., 1995. Ice cores as an index of global volcanism from 1850 to the present. Journal of Geophysical Research 100, 11549–11611.
Robock, A., Mao, J., 1995. The volcanic signal in surface temperature observations. Journal of Climate 8, 1086–1103.
Sato, M., Hansen, J., McCormick, M.P., Pollack, J., 1993. Stratospheric aerosol optical depth, 1850–1990. Journal of Geophysical Research 98.
Shepard, N., 1994. Partially non-Gaussian state-space models. Biometrika 81, 115–131.
Simkin, T., Siebert, L., 1994. Volcanoes of the World, 2nd edition. Geoscience Press, Tucson, 349 p.
Stark, H., Woods, J.W., 2002. Probability and Random Processes with Applications to Signal Processing, third ed. Prentice Hall, USA, New Jersey.
Stothers, R.B., 1996a. Major optical depth perturbations to the stratosphere from volcanic eruptions: pyrheliometric period, 1881–1960. Journal of Geophysical Research 101, 3901–3920, doi:10.1029/95JD03237.
Stothers, R., 1996b. The great dry fog of 1783. Climate Change 32.
Thordarson, T., Self, S., 2003. Atmospheric and environmental effects of the 1783–1784 laki eruption: a review and reassessment. Journal of Geophysical Research 108, doi:10.1029/2001JD002042.
Wahba, G., 1978. Improper priors, spline smoothing and the problem of guarding against model errors in regression. Journal of the Royal Statistical Society 40, 364–372.
Wastegard, S., Davies, S.M., 2009. An overview of distal tephrochronology in northern Europe during the last 1000 years. Journal of Quaternery Science 24, 500–512. doi:10.1002/jqs.1269.
Wecker, H., Ansley, C., 1983. The signal extraction approach to nonlinear regression and spline smoothing. Journal of the American Statistical Association 78, 81–89.
Wigley, T.M.L., Ammann, C., Santer, B.D., Raper, S., 2005. Effect of climate sensitivity on the response to volcanic forcing. Journal of Geophysical Research 110, doi:10.1029/2004JD005557.
Zielinski, G., 2000. Use of paleo-records in determining variability within the volcanism-climate system. Quaternary Science Reviews 19, 417–438.
Zielinski, G., Mayewski, P., Meeker, L., Whitlow, S., Twickler, M., Morrison, M., Meese, D., Gow, A., Alley, R., 1994. Record of volcanism since 7000 B.C. from the GISP2 Greenland ice core and implications for the volcano-climate system. Science 264, 948–952.